

**\*\*Volume Title\*\***

*ASP Conference Series, Vol. \*\*Volume Number\*\**

**\*\*Author\*\***

© **\*\*Copyright Year\*\*** *Astronomical Society of the Pacific*

## White Light Flare Continuum Observations with ULTRACAM

Adam F. Kowalski<sup>1</sup>, Mihalis Mathioudakis<sup>2</sup>, Suzanne L. Hawley<sup>1</sup>, Eric J. Hilton<sup>1</sup>, Vik S. Dhillon<sup>3</sup>, Tom R. Marsh<sup>4</sup>, Chris M. Copperwheat<sup>4</sup>

<sup>1</sup>*Astronomy Department, University of Washington Box 351580, Seattle, WA 98195, USA; adamfk@u.washington.edu*

<sup>2</sup>*Astrophysics Research Centre, School of Mathematics and Physics, Queen's University, Belfast BT7 1NN, UK*

<sup>3</sup>*Department of Physics, University of Sheffield, Sheffield S3 7RH, UK*

<sup>4</sup>*Department of Physics, University of Warwick, Gibbet Hill Rd, Coventry CV4 7AL, UK*

**Abstract.** We present sub-second, continuous-coverage photometry of three flares on the dM3.5e star, EQ Peg A, using custom continuum filters with WHT/ULTRACAM. These data provide a new view of flare continuum emission, with each flare exhibiting a very distinct light curve morphology. The spectral shape of flare emission for the two large-amplitude flares is compared with synthetic ULTRACAM measurements taken from the spectra during the large ‘megaflare’ event on a similar type flare star. The white light shape during the impulsive phase of the EQ Peg flares is consistent with the range of colors derived from the megaflare continuum, which is known to contain a Hydrogen recombination component and compact, blackbody-like components. Tentative evidence in the ULTRACAM photometry is found for an anti-correlation between the emission of these components.

### 1. Introduction

Active M dwarfs are notorious for white light flares in the near-UV and optical. White light emission is one of the first types of radiation to appear during both solar and stellar flares (Neidig & Kane 1993; Hawley et al. 1995) with a quickly-evolving impulsive phase followed by an extended decay phase that can sometimes last up to several hours (Hawley & Pettersen 1991; Kowalski et al. 2010a). Time-resolved spectral observations of M dwarf flares show a rising continuum into the near-UV, which has been modelled as a hot,  $T \sim 10,000$  K blackbody spectrum (Hawley & Fisher 1992; Fuhrmeister et al. 2008). Recent spectral observations have revealed that a Hydrogen recombination component (Balmer continuum) can also contribute significantly to the decay phase of the white light for  $\lambda < 3646\text{\AA}$  (Kowalski et al. 2010a).

Spectral observations can be severely limited by time resolution, with integration times (minutes) typically much longer than the timescales of flare evolution (seconds); as a result, broadband filters are more often used to characterize the time-evolution of the white light continuum. An analysis of 4 flares on the dM3e star AD Leo using UV+UBVR filters has shown a nearly isothermal  $T \sim 8500 - 10,000$  K component in

the white light at all times (Hawley et al. 2003). Another study by Zhilyaev et al. (2007) analyzed high time-cadence ( $\sim 0.1$ s) *UBVRI* photometry and concluded that multiple components (a Hydrogen recombination component and  $\sim 18,000$  K blackbody) contribute to varying degrees during a flare on the dM3.5e star EV Lac.

The origin of the white light continuum during flares is a long-outstanding problem in solar and stellar flare physics. The Allred et al. (2006) non-LTE radiative hydrodynamic (RHD) models of M dwarf flares predict two continuum sources, but the photosphere does not receive enough energy to generate the temperatures near  $\sim 10,000$  K implied by the observations. However, the model white light emission resembles the shape of a hot ( $T \sim 8900$  K) blackbody when convolved with the UV+*UBVR* filters (see Figure 12 of Allred et al. 2006), indicating that there might be a degeneracy in the measured flare shape when using broad filters that encompass numerous spectral lines and continua.

We have begun a flare monitoring campaign with ULTRACAM using custom continuum filters to characterize the white light continuum properties on sub-second timescales. In these proceedings, we present our first ULTRACAM observations of the flare star EQ Peg A.

## 2. Observations

ULTRACAM is an ultrafast, triple-beam, cascade dichroic CCD camera, and has helped open up simultaneous multiband, sub-second time domain astronomy (Dhillon et al. 2007). On UT 10 August 2008, we obtained flare observations of EQ Peg A and B using ULTRACAM on the 4.2-m William Herschel Telescope at La Palma. EQ Peg A and B are a resolved binary system consisting of dM3.5e and dM4.5e components, which have well-studied flare properties from the X-ray through the optical (Lacy et al. 1976; Robrade et al. 2004; Mathioudakis et al. 2006; Liefke et al. 2008).

The observations were taken with an  $H\alpha$  filter (FWHM  $\sim 50\text{\AA}$ ) in addition to two custom continuum filters, NBF3510 ( $\lambda_c \sim 3510\text{\AA}$ , FWHM  $\sim 100\text{\AA}$ ) and NBF4170 ( $\lambda_c \sim 4170\text{\AA}$ , FWHM  $\sim 50\text{\AA}$ ), designed specifically to avoid line emission and the Balmer jump at  $\lambda = 3646\text{\AA}$ . Figure 1 (left panel) shows a flare spectrum from Kowalski et al. (2010a) with the NBF3510, NBF4170, and Johnson *U* band transmission efficiencies. The *U* band contains high-order Hydrogen emission and straddles the Balmer jump whereas the custom filters effectively isolate the continuum emission. Exposure times were 0.291 s for the NBF3510 camera and 0.134 s for the NBF4170 and  $H\alpha$  cameras.

The data were reduced with the ULTRACAM pipeline software<sup>1</sup>, and we used a nearby comparison star, Gl 896 C, to obtain differential photometric measurements in all bands. A fixed aperture radius of 6 pixels was used. The night was photometric with variable seeing, and the observations were terminated due to morning twilight.

## 3. Light Curve Data

During the last  $\sim 30$  minutes of observations, EQ Peg A produced three flares, each with a unique light curve morphology (Figure 1, right panel): a ‘gradual’ flare (**G**) at

---

<sup>1</sup><http://deneb.astro.warwick.ac.uk/phsaap/software/ultracam/html>

$t \sim 50$  min, an ‘impulsive’ flare (**I**) at  $t \sim 64$  min, and a ‘traditional’ flare (**T**) at  $t \sim 70$  min. The high-cadence, continuous coverage photometry allows us to analyze the time-evolution of these flares without the ambiguity imposed by integration and readout times, which can be much greater than the timescales of flare evolution. We speculate that the differences in these light curve morphologies could be due to different active region structures (i.e., small vs. large arcades of flaring loops), different non-thermal particle beam flux evolution, and/or different white light continuum properties.

In general, each flare has similar morphologies in the NBF3510 and NBF4170 filters, and Table 1 summarizes the key properties. The **G** flare contains several emission peaks and a decay time that is long for its small peak amplitude. The **T** flare has a typical fast-rise, exponential-decay (‘FRED’) shape, but exhibits several variations from this trend. The **I** flare is nearly symmetric about the peak, but a low-amplitude, short decay is apparent when examined over a small time window. It is interesting that the **T** and **I** flares have similar peak amplitudes, but the **T** flare has nearly 5x the equivalent duration (energy) as the **I** flare.

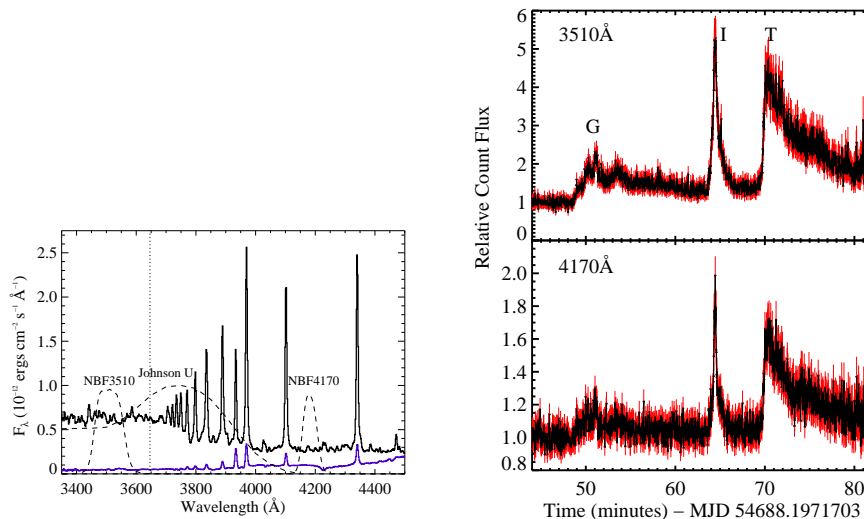


Figure 1. Left – Example flare (black) and quiescent (purple; scaled by a factor of 3) spectra from Kowalski et al. (2010a) with the transmission curves of the NBF3510, NBF4170, and the Maíz Apellániz (2006) Johnson U band. The Balmer jump wavelength is indicated by a vertical dotted line. Note that the flare-to-quiescent contrast is much greater in the NBF3510 filter. Right – Three flares on EQ Peg A in the NBF3510 and NBF4170 filters. We show every 4th point (top) and every 8th point (bottom) for clarity.

#### 4. Flare Color Analysis

If the underlying spectral energy distribution of the star is known, then the relative count light curves of Figure 1 (right panel) can be converted to a light curve of the spectral shape of the flare emission. Flux-calibrated M dwarf spectra near the atmospheric cut-off are rare, so we obtained deep 3400 - 5500Å spectra of EQ Peg A & B with the ARC

Table 1. NBF3510 Flare Properties

Flare type	peak amplitude ( $\sigma$ )	Decay Time Constant [min]	Equivalent Duration [min]
gradual ( <b>G</b> )	2.1 (0.1)	14	7.6
impulsive ( <b>I</b> )	5.1 (0.3)	1	3.2
traditional ( <b>T</b> )	4.3 (0.3)	7	14.8

3.5-m at the Apache Point Observatory in October, 2008. The spectra were reduced and flux-calibrated using standard IRAF<sup>2</sup> procedures. Following the spectrophotometry procedures of Sirianni et al. (2005) and Maíz Apellániz (2006), we estimate the ratio of quiescent fluxes of EQ Peg A in the NBF3510 and NBF4170 filters to be 0.40, with  $\sim 5\%$  uncertainty. If  $C(t)$  is the relative count flux (normalized to 1 during quiescence),  $C_o$  is the relative count flux immediately before the flare, and  $R_Q$  is the quiescent spectral ratio ( $F_{3510,Q}/F_{4170,Q}$ ), then the spectral shape of flare emission around the Balmer jump is

$$R_Q \times \frac{C_{3510}(t) - C_{o,3510}}{C_{4170}(t) - C_{o,4170}}. \quad (1)$$

This formula follows from the integrand of the equivalent duration (Gershberg 1972) for two filters, and we refer to it as the *flare color*.

#### 4.1. The Flare Color as a Proxy for Two Continuum Components

Recent spectral observations of a ‘megafare’ on the dM4.5e star, YZ CMi, revealed an anti-correlated time-evolution between the Balmer continuum (BaC) and a  $T \sim 10,000$  K blackbody continuum components (Kowalski et al. 2010a), which can be explained by a Balmer jump in absorption forming during the secondary flares (Kowalski et al. 2010b). Figure 2 shows how this flare would appear in the ULTRACAM continuum filters, using synthetic photometry and flare colors calculated from the spectra. The NBF3510 emission contains both blackbody and BaC components, whereas the NBF4170 contains primarily blackbody emission (and also probably a small amount of Paschen continuum; see Allred et al. (2006)). The anti-correlation between the total flare emission (U band, synthetic NBF3510, synthetic NBF4170) and the flare color is prominent throughout the entire decay and reflects the changing contributions of the blackbody and BaC components.

For fast time cadences not achievable with spectral measurements, the ULTRACAM flare color acts as a proxy for the relative contributions of the two white light continuum components. The flare color evolution is shown for the **I** and **T** flares in Figure 3. The errors are obtained by propagating the pipeline uncertainties, the standard deviation of the relative count flux in the preflare level, and the uncertainty in the quiescent spectral shape. The low-level flux enhancements during most of the flaring times lead to large errors for the original cadence. Binning the flare color into  $\Delta t = 3.8$  s bins allows for a time-resolved analysis during the flare peak times.

<sup>2</sup>IRAF is distributed by the National Optical Astronomy Observatories, which are operated by the Association of Universities for Research in Astronomy, Inc., under cooperative agreement with the National Science Foundation

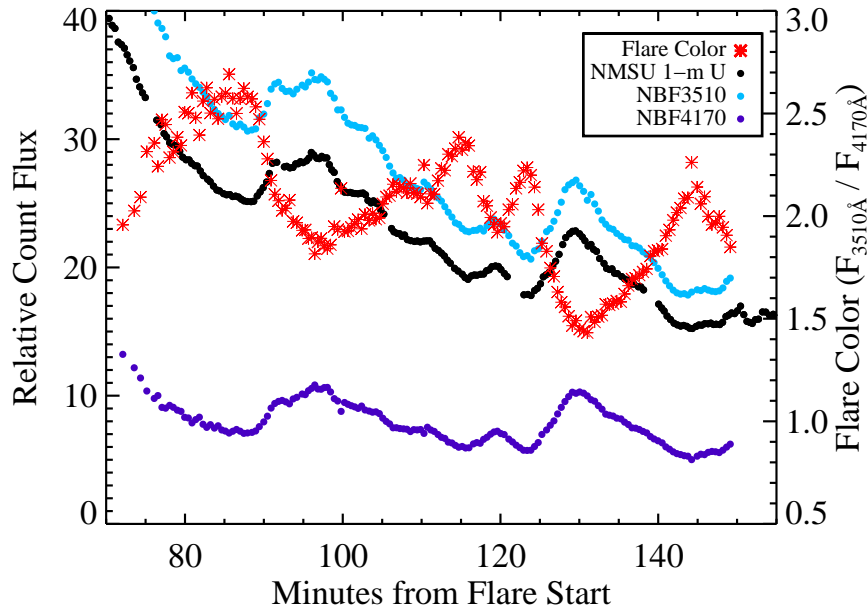


Figure 2. The U band light curve for 1.3 hrs of the megaflare on the dM4.5e star YZ CMi (see Kowalski et al. (2010a) for the complete light curve). From the simultaneous optical ARC 3.5-m spectra, we calculated synthetic NBF3510 and NBF4170 light curves and the flare color. An anti-correlation is prominent between the relative count fluxes and the color evolution. Note also the overall decline in flare color.

The flare colors of the **I** and **T** flares have several notable similarities to the megaflare. The average flare color around the main impulsive phase of the **I** and **T** flares is  $\sim 2.2$ , which falls within the range of flare colors derived from the megaflare spectra,  $\sim 1.5 - 2.5$ . The **I** and **T** flares have much smaller amplitudes than the megaflare, which was emitting at very high levels,  $\sim 40$  times the quiescent level, during the spectral observations. However, the similar flare colors imply a common geometrical scaling of the continuum components near the peaks of the **I** and **T** flares and during the decay phase of the megaflare, with the blackbody source having  $\sim 1/10$  the area of the BaC-emitting region.

We find tentative evidence for an anti-correlation between the flare color and the NBF3510 light curve at several times during the **I** and **T** flares. This is especially evident during the fast rise and fast decline phases of the **I** flare, which exhibit similar anti-correlated variations as in the secondary flares at  $t \sim 95$  min and  $\sim 130$  min in Figure 2. If all continuum components varied by the same factor (i.e., if the increasing flare flux resulted from scaled up emitting area of all components), then the flare color would be flat as a function of time. The changing flare color likely indicates the varying contributions of each continuum component, such that the blackbody has its largest relative contribution during the peak phase. Whether or not the decrease in flare color also results from the apparent amount of BaC emission decreasing as in the megaflare – due to increased Balmer continuum in *absorption* from the blackbody-like component

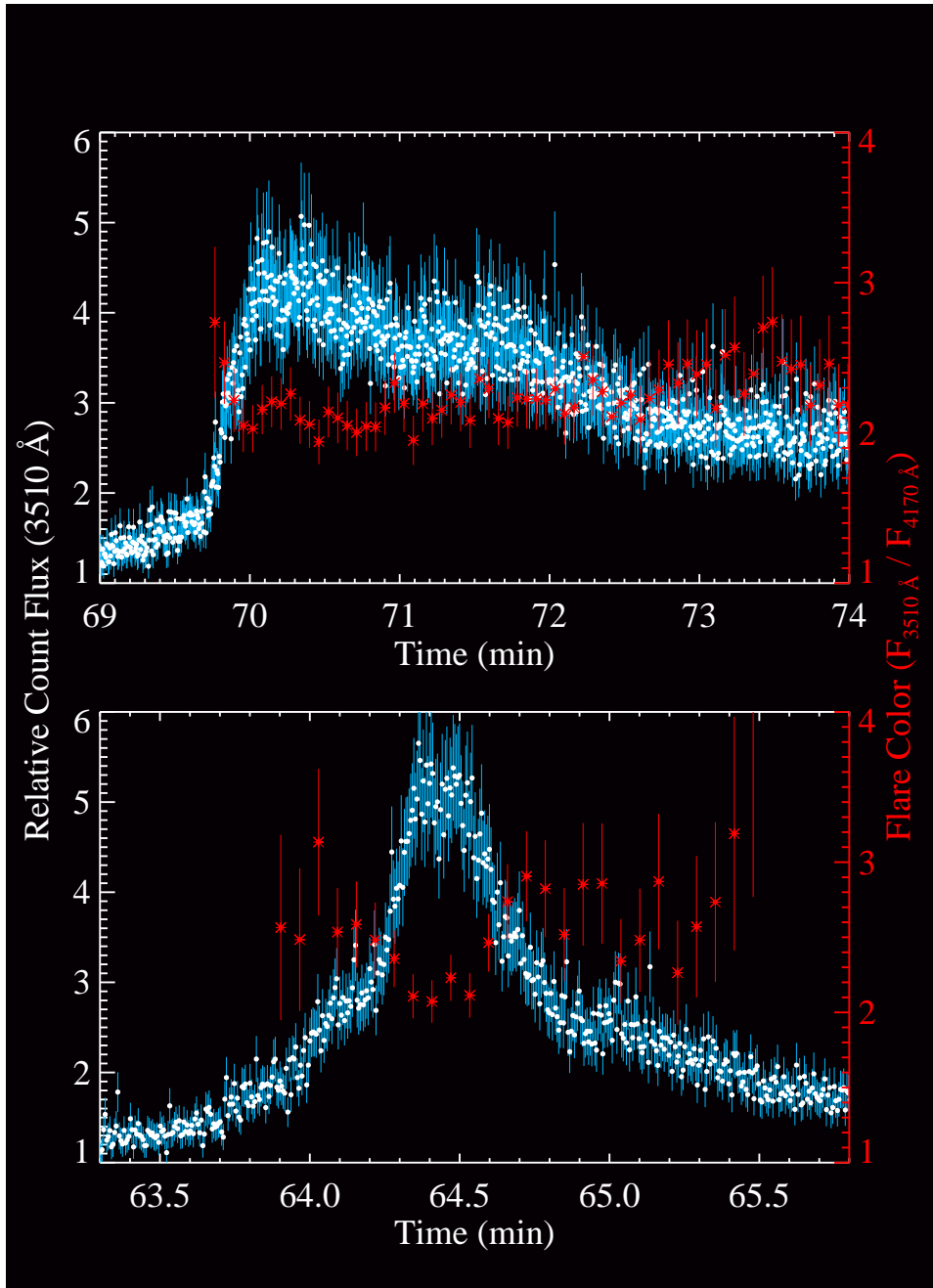


Figure 3. A closer view of the NBF3510 data for the **T** flare (top panel) and **I** flare (bottom panel) reveals a variety of substructure beyond a simple fast-rise, exponential decay shape. At this time-resolution, the rise in both flares has several distinct phases. The flare color is shown in red (right axis) and is binned by 3.8 s to reduce the errors. Note that the **T** flare has a decay phase that extends past the end of the observations at  $t \sim 83$  min.

(Kowalski et al. 2010b) – is difficult to determine from two-band photometry. Nonetheless, the observed flare color of  $\sim 2.2$  is consistent with this scenario.

Despite the similarities between the **I** and **T** flares and the megaflare, one can see that the flare color in Figure 2 exhibits an overall decrease, whereas a decreasing flare color is not found in the decay of the **I** and **T** flares. This inconsistency is not yet fully understood, but it may be related to the presence of several secondary (blackbody-like) flares during the megaflare decay.

#### 4.2. Comparison to Radiative Hydrodynamic Flare Models

We calculated NBF3510 and NBF4170 fluxes of the F11 flare spectrum from the Allred et al. (2006) RHD models and found that the model flare fluxes and colors are inconsistent with the observed and derived properties of the **I** and **T** flares. Given an extremely large flare that emits from 5% of the visible hemisphere (i.e., more than twice the inferred area of the BaC-emitting region during the megaflare), the model predicts relative peak fluxes that are only 2.0 and 1.07 in the NBF3510 and NBF4170 filters, respectively. The discrepancy is particularly noticeable for the amplitudes of the **I** and **T** flares. The **G** flare has an amplitude that is more consistent with the model; however, the required surface area coverage is likely not realistic for such a short-lived, weak flare. The flare color of the F11 model spectrum is  $\sim 5$ , which is also inconsistent with the observations. Increasing the area of the backwarmed photosphere, which might be a more realistic geometry for a flaring region (Isobe et al. 2007), would help to decrease the flare color of the model from such a discrepant value.

It is a known problem that the hot blackbody component of the white light continuum is not produced in the RHD flare models. These models may fall short in matching the observed properties of flares due to not having enough power in accelerated electrons, and/or they may be limited by the one-dimensional treatment of a process that often includes arcades of flare loops (see the spatial evolution of solar flare white light footpoints in Wang et al. 2007; Wang 2009).

### 5. Conclusions

We use ULTRACAM continuum observations of EQ Peg A to characterize white light flares with custom continuum filters that do not contain Hydrogen line contamination. A variety of flare light curve morphologies are observed on sub-second timescales, with all of these flares exhibiting substructure beyond the standard fast-rise, exponential decay (FRED) shape. The rate at which each flare shape occurs is not known, but such information would help to understand the physical parameters and conditions that cause, for example, an **I**-type flare to occur instead of a **T**-type flare.

We calculate a flare continuum color to quantify the spectral shape around the Balmer jump. The flare color evolution shows preliminary evidence of variations on timescales of several seconds during the impulsive phase. The average color over the first peak of these two EQ Peg flares is consistent with the synthetic flare colors during the decay phase of a megaflare on the M dwarf YZ CMi, for which we have spectra and therefore a detailed understanding of each continuum component. We find tentative evidence for an anti-correlated time-evolution between the relative flux and the flare color, similar to that previously presented for the YZ CMi flare.

These ULTRACAM observations show that it is possible to use the NBF3510 and NBF4170 filters as proxies to understand the components of the white light continuum

on timescales not accessible by spectral observations. Additional observations with ULTRACAM of larger flares (hence, well-measured flare colors) would provide a more precise determination of the flare color during all phases of the flare. More observations are also critical for finding and characterizing the properties of the anti-correlation between continuum components.

**Acknowledgments.** We are grateful to Robert Ryans (QUB) for installing and maintaining the ULTRACAM pipeline software. AFK acknowledges support from NSF grant AST 0807205. Based on observations obtained with the 4.2-meter William Herschel Telescope operated on the island of La Palma by the Isaac Newton Group in the Spanish Observatorio del Roque de los Muchachos of the Instituto de Astrofísica de Canarias, and observations with the Apache Point Observatory 3.5-meter telescope, which is owned and operated by the Astrophysical Research Consortium.

## References

- Allred, J. C., Hawley, S. L., Abbett, W. P., & Carlsson, M. 2006, *ApJ*, 644, 484. [arXiv:astro-ph/0603195](#)
- Dhillon, V. S., Marsh, T. R., Stevenson, M. J., Atkinson, D. C., Kerry, P., Peacocke, P. T., Vick, A. J. A., Beard, S. M., Ives, D. J., Lunney, D. W., McLay, S. A., Tierney, C. J., Kelly, J., Littlefair, S. P., Nicholson, R., Pashley, R., Harlaftis, E. T., & O'Brien, K. 2007, *MNRAS*, 378, 825. [0704.2557](#)
- Fuhrmeister, B., Liefke, C., Schmitt, J. H. M. M., & Reiners, A. 2008, *A&A*, 487, 293. [0807.2025](#)
- Gershberg, R. E. 1972, *Ap&SS*, 19, 75
- Hawley, S. L., Allred, J. C., Johns-Krull, C. M., Fisher, G. H., Abbett, W. P., Alekseev, I., Avgoloupis, S. I., Deustua, S. E., Gunn, A., Seiradakis, J. H., Sirk, M. M., & Valenti, J. A. 2003, *ApJ*, 597, 535
- Hawley, S. L., & Fisher, G. H. 1992, *ApJS*, 78, 565
- Hawley, S. L., Fisher, G. H., Simon, T., Cully, S. L., Deustua, S. E., Jablonski, M., Johns-Krull, C. M., Pettersen, B. R., Smith, V., Spiesman, W. J., & Valenti, J. 1995, *ApJ*, 453, 464
- Hawley, S. L., & Pettersen, B. R. 1991, *ApJ*, 378, 725
- Isobe, H., Kubo, M., Minoshima, T., Ichimoto, K., Katsukawa, Y., Tarbell, T. D., Tsuneta, S., Berger, T. E., Lites, B., Nagata, S., Shimizu, T., Shine, R. A., Suematsu, Y., & Title, A. M. 2007, *PASJ*, 59, 807. [0711.3946](#)
- Kowalski, A. F., Hawley, S. L., Holtzman, J. A., Wisniewski, J. P., & Hilton, E. J. 2010a, *ApJ*, 714, L98. [1003.3057](#)
- 2010b, *ArXiv e-prints*. [1010.0452](#)
- Lacy, C. H., Moffett, T. J., & Evans, D. S. 1976, *ApJS*, 30, 85
- Liefke, C., Ness, J., Schmitt, J. H. M. M., & Maggio, A. 2008, *A&A*, 491, 859. [0810.0150](#)
- Maíz Apellániz, J. 2006, *AJ*, 131, 1184. [arXiv:astro-ph/0510785](#)
- Mathioudakis, M., Bloomfield, D. S., Jess, D. B., Dhillon, V. S., & Marsh, T. R. 2006, *A&A*, 456, 323. [arXiv:astro-ph/0605196](#)
- Neidig, D. F., & Kane, S. R. 1993, *Solar Phys.*, 143, 201
- Robrade, J., Ness, J., & Schmitt, J. H. M. M. 2004, *A&A*, 413, 317. [arXiv:astro-ph/0310600](#)
- Sirianni, M., Jee, M. J., Benítez, N., Blakeslee, J. P., Martel, A. R., Meurer, G., Clampin, M., De Marchi, G., Ford, H. C., Gilliland, R., Hartig, G. F., Illingworth, G. D., Mack, J., & McCann, W. J. 2005, *PASP*, 117, 1049. [arXiv:astro-ph/0507614](#)
- Wang, L. 2009, *ApJ*, 694, 247
- Wang, L., Fang, C., & Ming-DeDing 2007, *ChJAA*, 7, 721
- Zhilyaev, B. E., Romanyuk, Y. O., Svyatogorov, O. A., Verlyuk, I. A., Kaminsky, B., Andreev, M., Sergeev, A. V., Gershberg, R. E., Lovkaya, M. N., Avgoloupis, S. J., Seiradakis, J. H., Contadakis, M. E., Antov, A. P., Konstantinova-Antova, R. K., & Bogdanovski, R. 2007, *A&A*, 465, 235